Langmuir
Article
pubs.acs.org/Langmuir

Immobilization and Molecular Interactions between Bacteriophage and Lipopolysaccharide Bilayers

Hitesh Handa,[†] Stephen Gurczynski,[‡] Matthew P. Jackson,[‡] and Guangzhao Mao*[,†]

[†]*Department of Chemical Engineering and Materials Science, and* [‡]*Department of Immunology and Microbiology, Wayne State University, Detroit, Michigan 48202*

Received April 5, 2010. Revised Manuscript Received May 5, 2010

The paper describes immobilization methods of bacteriophage P22 and tailspike gp9 proteins isolated from P22 on atomic force microscope (AFM) probes. The paper also reports single molecule force spectroscopy (SMFS) using AFM of the immobilized P22 (or gp9) interactions with substrate-supported O-antigenic lipopolysaccharides (LPS) bilayers. LPS covers the outer membrane of Gram-negative bacteria, such as *Salmonella typhimurium*. Evidence from AFM imaging and SMFS shows that immobilized P22 (or gp9) are capable of strong and multivalent binding to supported LPS. The most common rupture forces between P22 and LPS were identified to be 72, 130, 206, and 279 pN at force loading rate of 12 000 pN/s. The quantized unbinding force was found to decrease with decreasing force loading rate as predicted by the Bell model. By fitting the force data with the Bell model, an energy barrier of 55 kJ/mol was obtained. Evidence is also provided that demonstrates the resilience of phage to pH and temperature fluctuation as well as dehydration/rehydration cycles. The biospecific interactions between P22 and the LPS are relevant to cell infection, inflammation, cancer progression and metastasis, food safety, pharmaceuticals, and biosensor development.

1. Introduction

The original papers on single-bond rupture between avidin/strepdavidin and biotin[1,2] have led to advances in AFM force measurements (or SMFS) for the determination of adhesion/rupture/unbinding forces between ligand−receptor pairs. Molecular interactions between antigen−antibody,[3−7] complementary nucleotides,[8−10] and adhesion protein−receptor in cell adhesion[11−15] as well as conformational transitions during protein unfolding[16−18] have been measured by SMFS. Recent improvements in SMFS techniques include increased mobility of binding proteins affixed to the AFM probe through flexible tethers, restriction of the number of binding proteins on the AFM probe, and variation of force loading rates (dynamic SMFS) to yield energy landscapes of biological interactions.

Here we report AFM imaging and SMFS measurements of interactions between bacteriophage P22 tailspike proteins (TSPs) and O-antigenic lipopolysaccharides (LPS) of Gram-negative *Salmonella typhimurium S. enteritidis*, *S. typhi253Ty* (*S. typhimurium*). SMFS complements other techniques such as titration calorimetry,[19−21] surface plasmon resonance,[22] X-ray crystallography, and NMR spectroscopy[23] for the understanding of thermodynamics, adhesion, binding modes, and structural aspects of protein−carbohydrate interactions. The protein−carbohydrate interactions play the key role of regulating cell−cell recognition, including cell infection by bacteria and viruses, inflammation, and cancer progression and metastasis.[24−27] In addition, the knowledge on protein−carbohydrate interactions is relevant to food safety,[28] pharmaceuticals,[29] and biosensor development.[30,31] Previous SMFS studies on protein−carbohydrate interactions have been largely focused on the interactions between high-molecular-weight

*To whom correspondence should be addressed. E-mail: gzmao@eng.wayne.edu.

(1) Florin, E. L.; Moy, V. T.; Gaub, H. E. *Science* **1994**, *264* (5157), 415−−417.
(2) Lee, G. U.; Kidwell, D. A.; Colton, R. J. *Langmuir* **1994**, *10* (2), 354−357.
(3) Dammer, U.; Hegner, M.; Anselmetti, D.; Wagner, P.; Dreier, M.; Huber, W.; Guntherodt, H. J. *Biophys. J.* **1996**, *70* (5), 2437−2441.
(4) Hinterdorfer, P.; Baumgartner, W.; Gruber, H. J.; Schilcher, K.; Schindler, H. *Proc. Natl. Acad. Sci. U.S.A.* **1996**, *93* (8), 3477−3481.
(5) Ros, R.; Schwesinger, F.; Anselmetti, D.; Kubon, M.; Schafer, R.; Pluckthun, A.; Tiefenauer, L. *Proc. Natl. Acad. Sci. U.S.A.* **1998**, *95* (13), 7402−7405.
(6) Harada, Y.; Kuroda, M.; Ishida, A. *Langmuir* **2000**, *16* (2), 708−715.
(7) Idiris, A.; Kidoaki, S.; Usui, K.; Maki, T.; Suzuki, H.; Ito, M.; Aoki, M.; Hayashizaki, Y.; Matsuda, T. *Biomacromolecules* **2005**, *6* (5), 2776−2784.
(8) Lee, G. U.; Chrisey, L. A.; Colton, R. J. *Science* **1994**, *266* (5186), 771−773.
(9) Strunz, T.; Oroszlan, K.; Schafer, R.; Guntherodt, H. J. *Proc. Natl. Acad. Sci. U.S.A.* **1999**, *96* (20), 11277−11282.
(10) Boland, T.; Ratner, B. D. *Proc. Natl. Acad. Sci. U.S.A.* **1995**, *92* (12), 5297−5301.
(11) Dammer, U.; Popescu, O.; Wagner, P.; Anselmetti, D.; Guntherodt, H. J.; Misevic, G. N. *Science* **1995**, *267* (5201), 1173−1175.
(12) Vincent, D.; Claire, V.; Dominique, R.; Frank, L.; Yves, F. D. *ChemPhysChem* **2009**, *10* (9−10), 1672−1675.
(13) Wojcikiewicz, E. P.; Abdulreda, M. H.; Zhang, X.; Moy, V. T. *Biomacromolecules* **2006**, *7* (11), 3188−3195.
(14) Zhang, X.; Wojcikiewicz, E.; Moy, V. T. *Biophys. J.* **2002**, *83* (4), 2270−2279.
(15) Benoit, M.; Gabriel, D.; Gerisch, G.; Gaub, H. E. *Nat. Cell Biol.* **2000**, *2* (6), 313−317.
(16) Oberhauser, A. F.; Marszalek, P. E.; Erickson, H. P.; Fernandez, J. M. *Nature* **1998**, *393* (6681), 181−185.
(17) Rief, M.; Gautel, M.; Schemmel, A.; Gaub, H. E. *Biophys. J.* **1998**, *75* (6), 3008−3014.
(18) Oesterhelt, F.; Oesterhelt, D.; Pfeiffer, M.; Engel, A.; Gaub, H. E.; Muller, D. J. *Science* **2000**, *288* (5463), 143−146.
(19) Thomson, J.; Liu, Y. F.; Sturtevant, J. M.; Quiocho, F. A. *Biophys. Chem.* **1998**, *70* (2), 101−108.
(20) Baxa, U.; Cooper, A.; Weintraub, N.; Pfeil, W.; Seckler, R. *Biochemistry* **2001**, *40* (17), 5144−5150.
(21) Mandal, D. K.; Kishore, N.; Brewer, C. F. *Biochemistry* **1994**, *33* (5), 1149−1156.
(22) Smith, E. A.; Thomas, W. D.; Kiessling, L. L.; Corn, R. M. *J. Am. Chem. Soc.* **2003**, *125* (20), 6140−6148.
(23) Wormald, M. R.; Petrescu, A. J.; Pao, Y. L.; Glithero, A.; Elliott, T.; Dwek, R. A. *Chem. Rev.* **2002**, *102* (2), 371−386.
(24) Lis, H.; Sharon, N. *Chem. Rev.* **1998**, *98* (2), 637−674.
(25) Varki, A. *Glycobiology* **1993**, *3* (2), 97−130.
(26) Bertozzi, C. R.; Kiessling, L. L. *Science* **2001**, *291* (5512), 2357−2364.
(27) Ritchie, G. E.; Moffatt, B. E.; Sim, R. B.; Morgan, B. P.; Dwek, R. A.; Rudd, P. M. *Chem. Rev.* **2002**, *102* (2), 305−319.
(28) Samant, S. K.; Singhal, R. S.; Kulkarni, P. R.; Rege, D. V. *Int. J. Food Sci. Technol.* **1993**, *28* (6), 547−−562.
(29) Ooi, V. E. C.; Liu, F. *Curr. Med. Chem.* **2000**, *7* (7), 715−729.
(30) Handa, H.; Gurczynski, S.; Jackson, M. P.; Auner, G.; Walker, J.; Mao, G. *Surf. Sci.* **2008**, *602* (7), 1392−1400.
(31) Stewart, G. S. A. B.; Jassim, S. A. A.; Denyer, S. P.; Newby, P.; Linley, K.; Dhir, V. K. *J. Appl. Microbiol.* **1998**, *84* (5), 777−783.

polysaccharides and AFM probes modified by lectin, *e.g.*, concanavalinA (conA).[32−37] Rupture forces in the range of 20−100 pN were reported for single lectin−carbohydrate interactions. Because of the high molecular weights of the polysaccharides with rupture distances as large 1000 nm, the force vs. distance curves can be fitted to single chain deformation models, such as the freely jointed chain (FJC) model.

The study uses low-molecular-weight LPS, which covers ~45% of the outer membrane of Gram-negative bacteria.[38−40] The LPS molecule is comprised of lipid A, an inner and an outer core, and an outermost region of O-antigenic units. The inner core consists of L-glycero-D-manno-heptose residues linked to α-3-deoxy-D-manno-oct-2-ulosonic acid (Kdo). The inner core is linked to lipid A by Kdo. The outer core consists of an oligosaccharide (up to six sugar units). Bacteriophage P22 is known to bind to the repetitive O-antigenic part of the LPS outer membrane in *S. typhimurium*. There are three types of hosts, namely A, B, and D1 serotypes. All the serotypes share a common trisachharide repeating unit α-D-mannose-(1-4)-α-L-rhamnose-(1−3)-α-D-galactose for the O antigen part and differ in the branching carbohydrate, a 3,6-dideoxyhexose α-(1-3)-linked to D-mannose. Dideoxyhexoses are paratose for serogroup A, abequose for serogroup B, and tyvelose for serogroup D1. The branching dideoxyhexose unit gives specificity to the interaction. The *S. typhimurium* used here possesses O-antigenic serogroup B.[41−43]

Phage P22 consists of double-stranded DNA packaged in an icosahedral capsid head and the O-antigen recognizing TSPs.[41,44−46] Up to 6 TSP gp9 (6 × 215.4 kDa) copies are noncovalently attached to the capsid head by the N-terminal domain of gp9 while its C-terminal domain binds to the cellular LPS. The main TSP is a right-handed parallel β-helix of 13 complete turns. The binding site is located in the central part of the β-helix, i.e., approximately 80 Å from the C terminus.[42,43] The cross-section of the β-helix is approximately triangular where the binding cleft is formed by a 63-residue domain on one side and three smaller insertions of 5−25 residues on the other side. The length and the width of the binding cleft are approximately 21 and 8−13 Å, respectively.[42,43,47]

To study the molecular interactions between phage and bacteria, P22 was immobilized on an AFM probe and the LPS bilayer was deposited on solid substrate by vesicle fusion (Figure 1a). P22 was attached to the AFM probe via organosilane-based bioconjugation chemistry. Alternatively, gp9 proteins extracted from the P22 capsid were attached to the AFM probe by reacting with a carbosilane using bioconjugation chemistry. Both AFM imaging and SMFS were conducted in aqueous solution. The force vs distance curves display one or multiple local adhesion force minima during probe retraction suggesting one or multiple unbinding events between P22 and LPS. The force curves were measured at different force loading rates and analyzed using the Bell model.[48] The interactions were measured at different pH and temperature values and after a dehydration and rehydration cycle in order to test the tolerance of P22 to environment stresses.

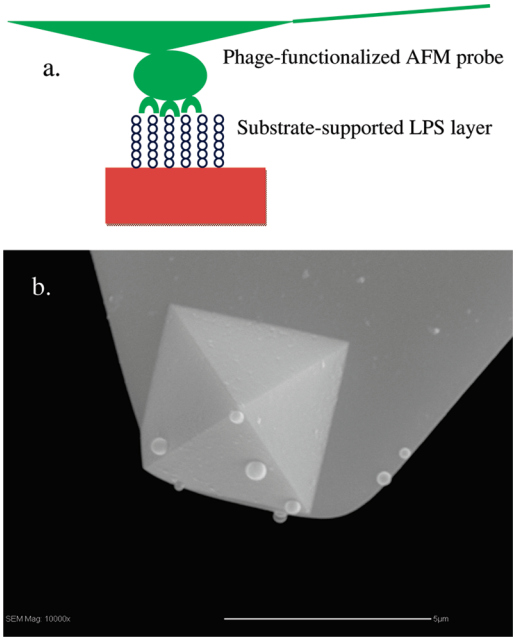

Figure 1. (a) Schematic representation of unbinding forces measured between phage P22 modified AFM probe and substrate-supported LPS bilayer. (b) SEM image of P22-coated AFM probe. The bar length is 5 μm.

2. Experimental Section

Materials. 3-Aminopropyltrimethoxysilane (APTMS), o-phenylenediamine dihydrochloride (OPD), polyethylenimine (PEI, 25 kDa), and LPS from *Salmonella enterica serotype typhimurium* (purified by phenol extraction) were purchased from Sigma-Aldrich. 10-(Carbomethoxy)decyldimethylchlorosilane (CDDMS) was purchased from Gelest. *N*-hydroxysulfosuccinimide (sulfo-NHS) and 1-ethyl-3-(3-dimethylaminopropyl) carbodiimide hydrochloride (EDC) were purchased from Pierce. Horseradish peroxidase (HRP)-labeled anti *Salmonella* IgG and anti *E. coli* IgG were purchased from U.S. Biological (s0060-20) and HRP-labeled anti *Listeria* IgG was purchased from Abcam (ab20357). Phage P22 (*Salmonella enterica subsp. Enterica serovar typhimurium* bacteriophage) ATCC (19585-B1) and *S. typhimurium* ATCC (19585), and *E. coli* strain ATCC (33780) were used. Cellulose acetate filters (0.22 μm) were purchased from Corning. Grade V5 muscovite mica sheets were purchased from Ted Pella and hand cleaved just before use. Deionized water from Barnstead Nanopure water purification system (resistivity 18 MΩ × cm) was used to prepare all solutions.

Bacteria Culture. A 3 mL portion of Luria−Bertani (LB broth) was added to a 15 mL centrifuge tube. The medium was inoculated with *S. typhimurium*. The tube was shaken in a water bath at 37 °C overnight. Cells were removed from the bath in log

(32) Ludwig, M.; Rief, M.; Schmidt, L.; Li, H.; Oesterhelt, F.; Gautel, M.; Gaub, H. E. *Appl. Phys. A* **1999**, *68* (2), 173−176.
(33) Francius, G.; Alsteens, D.; Dupres, V.; Lebeer, S.; De Keersmaecker, S.; Vanderleyden, J.; Gruber, H. J.; Dufrene, Y. F. *Nat. Protoc.* **2009**, *4* (6), 939(8).
(34) Marszalek, P. E.; Li, H. B.; Fernandez, J. M. *Nat. Biotechnol.* **2001**, *19* (3), 258−262.
(35) Touhami, A.; Hoffmann, B.; Vasella, A.; Denis, F. A.; Dufrene, Y. F. *Microbiology* **2003**, *149* 2873−2878.
(36) Ratto, T. V.; Rudd, R. E.; Langry, K. C.; Balhorn, R. L.; McElfresh, M. W. *Langmuir* **2006**, *22* (4), 1749−1757.
(37) Targosz, M.; Czuba, P.; Biedron, R.; Strus, M.; Gamian, A.; Marcinkiewicz, J.; Szymonski, M. *Acta Phys. Pol., A* **2006**, *109* (3), 421−426.
(38) Caroff, M.; Karibian, D. *Carbohydr. Res.* **2003**, *338* (23), 2431−2447.
(39) DiRienzo, J. M.; Nakamura, K.; Inouye, M. *Annu. Rev. Biochem.* **1978**, *47* (1), 481−532.
(40) Kotra, L. P.; Golemi, D.; Amro, N. A.; Liu, G.-Y.; Mobashery, S. *J. Am. Chem. Soc.* **1999**, *121* (38), 8707−8711.
(41) Baxa, U.; Steinbacher, S.; Miller, S.; Weintraub, A.; Huber, R.; Seckler, R. *Biophys. J.* **1996**, *71* (4), 2040−2048.
(42) Steinbacher, S.; Baxa, U.; Miller, S.; Weintraub, A.; Seckler, R.; Huber, R. *Proc. Natl. Acad. Sci. U.S.A.* **1996**, *93* (20), 10584−10588.
(43) Steinbacher, S.; Miller, S.; Baxa, U.; Budisa, N.; Weintraub, A.; Seckler, R.; Huber, R. *J. Mol. Biol.* **1997**, *267* (4), 865−880.
(44) Jiang, W.; Li, Z. L.; Zhang, Z. X.; Baker, M. L.; Prevelige, P. E.; Chiu, W. *Nat. Struct. Biol.* **2003**, *10* (2), 131−135.
(45) Israel, V.; Rosen, H.; Levine, M. *J. Virol.* **1972**, *10* (6), 1152−1158.
(46) Andrews, D.; Butler, J. S.; Al-Bassam, J.; Joss, L.; Winn-Stapley, D. A.; Casjens, S.; Cingolani, G. *J. Biol. Chem.* **2005**, *280* (7), 5929−5933.
(47) Baxa, U.; Steinbacher, S.; Weintraub, A.; Huber, R.; Seckler, R. *J. Mol. Biol.* **1999**, *293* (3), 693−701.
(48) Bell, G. I. *Science* **1978**, *200* (4342), 618−627.

phase at a titer of approximately 10^6-10^7 cfu/mL. Freshly prepared overnight-cultured bacteria (100 μL) was added to each well of the 96-well plate containing gp9 or P22 coated substrates. The bacteria culture was allowed to react for 15 min at room temperature followed by a thorough wash with phosphate buffered saline (PBS, pH 7.2). As a control, freshly prepared overnight culture (100 μL) was added directly to the wells containing silanized glass without any gp9 or P22. In addition, *E. coli* strain 33780 and a Gram-positive bacterium, *L. monocytogenes*, was used as control. Freshly prepared overnight culture of *E. coli* and *L. monocytogenes* (100 μL, 10^6-10^7 cfu/mL) was added on gp9-coated glass for 15 min at 37 °C and subsequently washed with PBS before imaging.

P22 stock solution (12 mL, $\sim10^8$ pfu/mL) was placed in ultracentrifuge tube (13 mL). The solution was spun at 35 000 rpm in a Beckman SW41-Ti rotor for 2 h. After centrifugation a small transparent pellet could be faintly observed on the bottom of the tube. The pellet was then resuspended in distilled deionized water (1 mL) with an added $CaCl_2$ (2 mM) to stabilize the phage heads. The concentration of the final solution was $10^{10}-10^{12}$ pfu/mL. We found a diluted solution of 10^6-10^8 pfu/mL to be appropriate for P22 immobilization on the AFM probe for discrete unbinding force measurements.

Gp9 Separation. To measure the molecular interactions using only gp9 proteins instead of the whole P22, we first extracted P22 nucleic acid. Purified P22 (12 mL, $\sim10^{10}$ pfu/mL) was pelleted by ultracentrifugation at 35 000 rpm for 2 h in a Beckman tiSW-41 rotor. The supernatant was discarded, and the pellet was resuspended in 0.5 mL of lysis buffer (25 mM Tris pH 8.0, 10 mM EDTA, 100 mM NaCl, 0.5% SDS) and incubated overnight at room temperature. The next day 1 mL of phenol, equilibrated to 65 °C, was added to the phage solution which was then centrifuged for 3 min at 13 000 rpm in an Eppendorf tabletop centrifuge. The upper phase was then aspirated to a new tube and washed 3 times with 0.5 mL of 65 °C phenol. The upper phase was centrifuged and aspirated to a new tube after each wash. After the final phenol wash, three additional washes with 0.5 mL of 24:1 chloroform/isoamyl alcohol were performed with the top phase being centrifuged at 13 000 rpm and aspirated to a new tube in between washes. The top phase was then placed in 95% ethanol (three times the volume) at −80 °C for 1 h to precipitate the DNA. The precipitated DNA was then centrifuged for 30 min at 13 000 rpm to pellet the DNA. After aspirating off the ethanol the pellet was air-dried and resuspended in 50 μL of 10 mM Tris and 1 mM EDTA.

P22 gp9 proteins were then cloned from the P22 DNA. PCR was conducted using the DNA extracted from P22 using primers, forward CACCTACGATCCAGATCAA, and reverse CTAAAGTGTTGCCAAGGTTAA, to amplify the C-terminal 559 amino acids of the P22 TSP using a 30 cycle PCR program including 1 min denaturing at 94 °C, 1 min annealing at 54 °C, 2 min extension at 68 °C, and a final 7 min extension at 68 °C. The PCR product was visualized by ethidium bromide staining on a 0.8% agarose gel, and a band of ~1680 bp was observed (data not shown).

The amplified gp9 fragment was then ligated, following the manufacturer's instructions, into a pET100 Topo plasmid (Invitrogen), which added an N-terminal 6 × polyhistadine tag. The plasmid construct was then transformed, following manufacturer's instructions, into Invitrogen DE3 chemically competent *E. coli* cells. A 50 mL culture of *E. coli* containing the recombinant plasmid was then induced to express the gp9 fragment by inducing with 2 mM (isopropyl beta-D-thiogalactoside) (IPTG) for 5 h at 30 °C.

Recombinant gp9 was recovered from the polyhistidine tag using a Nickel agarose column (Ni-NTA purification system, Invitrogen). In short, 50 mL of induced *E. coli* culture was first clarified by centrifuging for 10 min at 8000 rpm in a sorval GSA rotor. The pellet was resuspended in 8 mL of native condition binding buffer (250 mM NaH_2PO_4 pH 8.0, 2.5 M NaCl). An 8 mg portion of lysozyme was added, and the mixture was placed on ice for 30 min. Cells were then sonicated in six 10 s bursts with a 10 s cooling off in between each burst. The lysate was then centrifuged in a sorval ss-34 rotor at 5000 rpm for 15 min to pellet cellular debris. The clarified lysate was then passed over a Ni-NTA column packed with 1.5 mL of nickel agarose slurry and washed and eluted per manufacturer's instructions. Fractions of 1 mL were obtained, and the purified protein was verified by Coomassie blue visualization on a 10% polyacrylamide gel.

AFM Probe Functionalization with P22 and gp9. Proper AFM probe functionalization is critical for the measurement of discrete unbinding forces between ligand and receptor pairs. Both alkylsilane[5,49−51] and alkylthiol[52−54] chemistries have been used to functionalize AFM probes. To enhance the motional freedom of proteins for increased chance of binding, spacer chemistry[4,55,56] has been extensively used. These studies have shown that 6−8 nm long spacers are sufficient for improving binding probability. Here we show that P22 (diameter ~70 nm) and gp9 protein (length ~15 nm)[43] are large enough for LPS binding.

We adopted the sulfo-NHS/EDC bioconjugation method[57−61] to attach gp9 to the AFM probe by linking the carboxylic acid group on gp9 with the amine group on the organosilane monolayer covering the AFM probe. We used the same method developed earlier for P22 immobilization on flat oxidized silicon or glass substrate.[30] The probe functionalization procedure is discussed briefly. Prior to the organosilane deposition, AFM probes were oxidized in a saturated solution of potassium hydroxide and ethanol for approximately 2 min followed by rinsing in ethanol (200 proof, Aaper). The monolayer of APTMS was deposited on the AFM probe by chemical vapor deposition (CVD).[30,62] Prior to CVD, the deposition chamber, a glass desiccator, was passivated by APTMS deposition. The silanization was carried out in the desiccator by exposing the AFM probe to APTMS for 15 min at 0.67 kPa followed by 16 h standing time under vacuum. The probe was subsequently rinsed in deionized water and ethanol and dried. To check the quality of the APTMS film, a piece of silicon nitride (1 × 1 cm^2) was placed in the same desiccator along with the probe. The water contact angle on the silanized substrate was measured to be approximately 62°.[63−67]

To functionalize the AFM probe with only the TSP portion of P22, the LPS-binding gp9 proteins were separated from the P22

(49) Chowdhury, P. B.; Luckham, P. F. *Colloids Surf. A* **1998**, *143* (1), 53−57.
(50) Headrick, J. E.; Berrie, C. L. *Langmuir* **2004**, *20* (10), 4124−4131.
(51) Xu, X. M.; Ikai, A. *Biochem. Biophys. Res. Commun.* **1998**, *248* (3), 744−748.
(52) Green, J. B. D.; Lee, G. U. *Langmuir* **2000**, *16* (8), 4009−4015.
(53) Han, T.; Williams, J. M.; Beebe, T. P. *Anal. Chim. Acta* **1995**, *307* (2−3), 365−376.
(54) Vezenov, D. V.; Zhuk, A. V.; Whitesides, G. M.; Lieber, C. M. *J. Am. Chem. Soc.* **2002**, *124* (35), 10578−10588.
(55) Riener, C. K.; Kienberger, F.; Hahn, C. D.; Buchinger, G. M.; Egwim, I. O. C.; Haselgrubler, T.; Ebner, A.; Romanin, C.; Klampfl, C.; Lackner, B.; Prinz, H.; Blaas, D.; Hinterdorfer, P.; Gruber, H. J. *Anal. Chim. Acta* **2003**, *497* (1−2), 101−114.
(56) Haselgrubler, T.; Amerstorfer, A.; Schindler, H.; Gruber, H. J. *Bioconjugate Chem.* **1995**, *6* (3), 242−248.
(57) Lahiri, J.; Isaacs, L.; Tien, J.; Whitesides, G. M. *Anal. Chem.* **1999**, *71* (4), 777−790.
(58) Patel, N.; Davies, M. C.; Hartshorne, M.; Heaton, R. J.; Roberts, C. J.; Tendler, S. J. B.; Williams, P. M. *Langmuir* **1997**, *13* (24), 6485−6490.
(59) Su, X.-L.; Li, Y. *Biosens. Bioelectron.* **2004**, *19* (6), 563−574.
(60) Campbell, G. A.; Mutharasan, R. *Biosens. Bioelectron.* **2005**, *21* (4), 597−607.
(61) Fung, Y. S.; Wong, Y. Y. *Anal. Chem.* **2001**, *73* (21), 5302−5309.
(62) Dong, J.; Wang, A.; Ng, K. Y. S.; Mao, G. *Thin Solid Films* **2006**, *515* (4), 2116−2122.
(63) Lee, I.; Wool, R. P. *Thin Solid Films* **2000**, *379* (1−2), 94−100.
(64) Wei, Z. Q.; Wang, C.; Zhu, C. F.; Zhou, C. Q.; Xu, B.; Bai, C. L. *Surf. Sci.* **2000**, *459* (3), 401−412.
(65) Faucheux, N.; Schweiss, R.; Lutzow, K.; Werner, C.; Groth, T. *Biomaterials* **2004**, *25* (14), 2721−2730.
(66) Wu, B.; Mao, G. Z.; Ng, K. Y. S. *Colloids Surf., A* **2000**, *162* (1−3), 203−213.
(67) Heise, A.; Stamm, M.; Rauscher, M.; Duschner, H.; Menzel, H. *Thin Solid Films* **1998**, *329* 199−203.

capsid portion and cross-linked to the AFM probe. To orient the gp9 protein so that its N-terminal domain is anchored on the probe while its C-terminal domain is free to bind to LPS, the AFM probe was functionalized with CDDMS using the same CVD procedure. The hydrolysis of ester to carboxylic acid was conducted with 1 M HCl for 1 h at room temperature, followed by rinsing with deionized water and nitrogen drying. The water contact angle on a simultaneously treated glass substrate was measured to be approximately 30°.[68]

To react P22 to the APTMS layer or gp9 to CDDMS, 2.2 mg of sulfo-NHS and 0.8 mg of EDC were added to each 1 mL aliquot of concentrated P22 (or gp9) solution. The samples were mixed briefly and allowed to react for 30 min at room temperature; 100 μL of P22 was then pipetted to cover the APTMS-terminated probe surface and the incubation was conducted overnight at 4 °C in microtiter plates. The P22-functionalized probe was imaged by SEM (Figure 1b). The P22 concentration was adjusted to 10^6-10^8 pfu/mL in order to yield the result shown. In the SEM image, the average particle diameter is 210 ± 50 nm, which is approximately 2−3 times the value reported in literature.[44] We attribute the discrepancy to an increase in diameter due flattening upon surface adsorption and drying as reported by others.[30]

Similarly, gp9 was reacted to carboxylic acid terminated glass chips (4×4 mm^2). The CDDMS-treated glass chips were first placed in a 1 M HCl bath for 1 h to activate the surface. The chips were washed with sterile distilled water and placed directly into a 1.5 mL Eppendorf tube containing 1 mL of purified gp9 and 1.1 mg of sulfo-NHS and 0.8 mg of EDC. The tube was vortexed vigorously for 1 min on max setting and incubated for 4 h at room temperature with shaking. The chips were extracted with forceps and placed activated side up in a 96-well microtiter plate. The gp9 solution (100 μL) was pipetted onto each well, and the plate was incubated overnight at 4 °C.

LPS Bilayer Formation by Vesicle Fusion. Multilamellar vesicles (MLVs) of LPS were prepared by adding 1 mg LPS to 1 mL of 25 mM KCl and 5 mM Hepes buffer (pH 7.4), vortexing for 1 min followed by incubation at 60 °C for 1 h. Sonicated unilamellar vesicles (SUVs) were prepared by sonicating the MLVs for 10 cycles of 4 min duration (2 min sonication and 2 min standby) at 40 W with 19 mm flat tip probe sonicator (Sonicator 3000, Misonix). To sediment any remaining MLVs and titanium particles detached from the probe the dispersion was centrifuged at 14 000 rpm for 30 min (Eppendorf 5810 R). The supernatants containing the SUVs were stored at 4 °C and used to make the supported LPS bilayer.

The supported LPS bilayer was created on a PEI-coated mica surface using a vesicle fusion method.[69−71] We follow closely the method developed by Tong and McIntosh. The mica sheet was dip-coated in 25 mM PEI solution in deionized water for 30 min followed by three 5 min rinses with deionized water in a bath sonicator (Branson 1510). The LPS molecule interacts electrostatically with the PEI layer deposited on the mica. A SUV suspension (150 μL) was applied onto freshly prepared PEI-coated mica surface. The LPS vesicles were allowed to adsorb and fuse on the surface at 60 °C for 3 h followed by rinsing with the buffer (Hepes and KCl).

Characterization. AFM images were obtained with Digital Instruments Nanoscope IIIa E scanner ($10 \times 10 \times 2.5$ μm^3 scan range). *In situ* AFM imaging was conducted in the liquid tapping mode (oscillating frequency ≈ 8 kHz, line scan rate = 2−3 μm/s) using silicon nitride probes (NP, VEECO) with a nominal radius of curvature of 20 nm. AFM height images are presented unless specified. Height images were plane-fit in the fast scan direction with no additional filtering operation. The surface roughness was determined using the root-mean-square surface roughness $R_q = \sqrt{\sum \frac{z_i^2}{n}}$ where z_i is the height value and n is the number of pixels in the image. Force-versus-distance curves were obtained in the liquid contact mode using the force calibration command. The force curves were converted from deflection-versus-z position data by defining the zero force and zero separation point.[72] The force loading rate, r_f in pN/s, is the product of the cantilever spring constant, k in pN/nm, and the scanner retraction speed, v in nm/s. The retraction speed was varied from 60 to 400 nm/s. A typical spring constant value, ~0.035 N/m, was determined by measuring the resonance frequency with 5% relative error and 20% absolute error.[73] The unbinding events are indicated by the sawtooth pattern in the retraction force curve. The unbinding force histograms were compiled from 50−100 force curves and were fitted with the Gaussian function. The effect of temperature variation on P22−LPS binding was studied by varying the solution temperature from room temperature to 60 °C using a thermal controller (model 2216e, Eurotherm). The heating unit, placed directly under the AFM fluid cell but isolated from the scanner by a spacer block, allows rapid changes (approximately 4 °C/min for heating and 2 °C/min for cooling) of the solution temperature in the fluid cell. The AFM scanner was calibrated separately when used with the thermal controller.

The functionalized AFM probes were imaged by SEM (Hitachi S-2400) at 25 kV. The AFM probes were sputtered for 30−60 s with gold for SEM analysis. EffaCoater (Ernest F. Fullam) was used for sputtering in vacuum (P = 200 mTorr) with a sputtering current of 50−100 mA.

The surface hydrophobicity was measured with an NRL contact angle goniometer (model 100, Rame-Hart) in the laboratory atmosphere. A 20 μL water droplet was placed on the substrate, and the static contact angles were measured on both sides of the droplet with a typical error of ±3°. Three droplets were placed at various spots on the substrate and the average readings are reported.

ELISA provides the value of relative amount of bacteria attached to gp9. After *S. typhimurium* is bound to gp9 the chips were incubated with 100 μL of a 3 w/w% bovine serum albumin (BSA) and 0.05 v/v% tween-20 in PBS solution for 30 min at 37 °C. This solution acts as a blocking agent to reduce nonspecific binding of the labeled antibody in the next step. After 30 min of incubation the chips were washed 40 times with a 0.05% tween-20 PBS solution in order to remove any excess blocking agent and unbound bacteria. Anti-*Salmonella* or anti-*Listeria* HRP-labeled antibodies were used depending on the experiment. The antibodies were diluted 10^3 times with 3% BSA/0.05% Tween-20 solution before use. The chips containing *S. typhimurium* or the control bacteria *E. coli* or *Listeria* attached to gp9 were incubated with HRP-labeled antibody (100 μL) for 1 h at 37 °C. The chips were washed thoroughly with 0.05% Tween-20 and PBS, respectively. OPD peroxidase was used as the ELISA substrate. Tablets of the substrate were dissolved in 20 mL deionized water. The substrate solution (200 μL) was allowed to react for 30 min at room temperature. Finally, the absorbance was measured at 450 nm using a microtiter plate spectrophotometer (Bio-Tek instruments EL340).

3. Results

The PEI-functionalized mica substrate was imaged by AFM in the tapping mode in air. The surface is devoid of aggregates and exhibits surface roughness $R_q = 0.3$ nm. The subsequently deposited LPS bilayer by vesicle fusion was imaged by AFM in the liquid tapping mode. Imaging in buffer (KCl, Hepes, pH 7.4) and deionized water (pH 5.5) yielded a similar surface feature.

(68) Gustavsson, J.; Altankov, G.; Errachid, A.; Samitier, J.; Planell, J. A.; Engel, E. *J. Mater. Sci., Mater. Med.* **2008**, *19* (4), 1839−1850.
(69) Brian, A. A.; Mcconnell, H. M. *Proc. Natl. Acad. Sci. U.S.A., Biol. Sci.* **1984**, *81* (19), 6159−6163.
(70) Shao, Z.; Mou, J.; Czajkowsky, D. M.; Yang, J.; Yuan, J. Y. *Adv. Phys.* **1996**, *45* 1−86.
(71) Tong, J. H.; McIntosh, T. J. *Biophys. J.* **2004**, *86* (6), 3759−3771.
(72) Liang, X. M.; Mao, G. Z.; Ng, K. Y. S. *Colloids Surf., B* **2004**, *34* (1), 41−51.
(73) Cleveland, J. P.; Manne, S.; Bocek, D.; Hansma, P. K. *Rev. Sci. Instrum.* **1993**, *64* (2), 403−405.

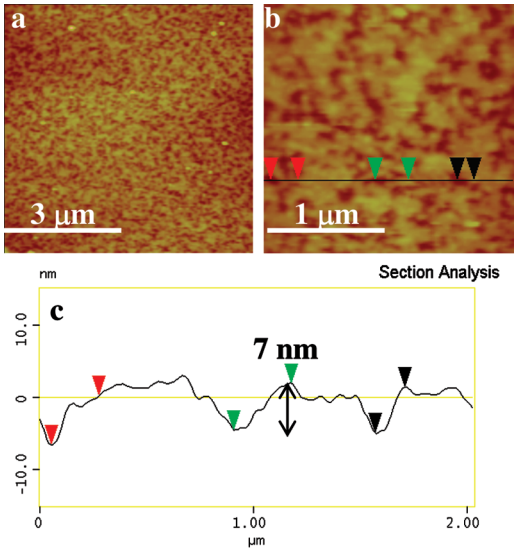

Figure 2. In-situ AFM height images of (a) LPS bilayer on PEI-coated mica (z range = 30 nm); (b) a closer look at the LPS bilayer (z range = 30 nm); (c) the cross-sectional height profile along the line in panel b showing the height of the bilayer to be 7 nm.

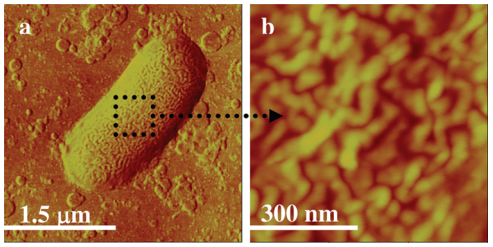

Figure 3. AFM images of *S. typhimurium*: (a) height image (z range = 90 nm); (b) phase image (z range = 10°). .

Figure 2a,b are typical images of the supported LPS bilayer. Figure 2a shows the film coverage to be uniform at the micrometer length scale. Figure 2b gives a closer view of the surface whose height profile is shown in Figure 2c. The LPS film thickness as determined from the sectional height analysis is 7 nm.[71] The film coverage is estimated by the bearing area analysis command (Nanoscope version 5.30, VEECO). The bearing area gives the percentage of the surface above the chosen reference plane, which is the substrate. The coverage is estimated to be ~80%, somewhat less than that reported by Tong et al.[71]

How does the bilayer surface compare to the native LPS layer of *S. typhimurium*? Figure 3 shows the morphology of a whole bacterium. *S. typhimurium* has a distinctive rodlike shape with length = 2 ± 0.3 μm, width = 790 ± 70 nm, and height = 185 ± 15 nm (Figure 3a). The domains on the whole bacterium are smaller and more tightly spaced than the LPS bilayer deposited on PEI-modified mica. The domain shape appears to be similar between the reconstituted and native one.

Another method to determine the LPS film thickness is to measure the force-versus-distance profiles during the approach of the LPS-coated substrate to an unmodified AFM probe. A typical approaching force curve between an AFM probe and a supported LPS bilayer is shown in Figure 4. The difference between the force onset distance, 18 nm, obtained at 0.1 nN, and the point of rapid force increase after the "jump-in", 3 nm, provides an estimation of the LPS bilayer thickness. The film thickness from the force curves, 15 nm, is higher than that estimated from the AFM sectional height analysis, 7 nm. The film likely experienced a

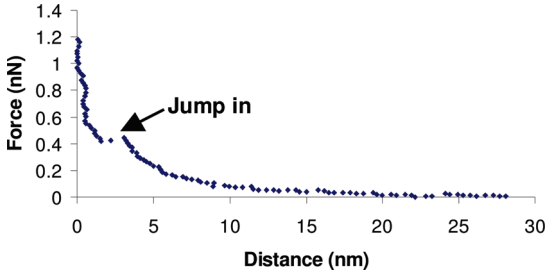

Figure 4. Force vs distance curve during approach of bare AFM probe toward the LPS bilayer. The mechanical instability point of the cantilever is marked as the "jump-in" point.

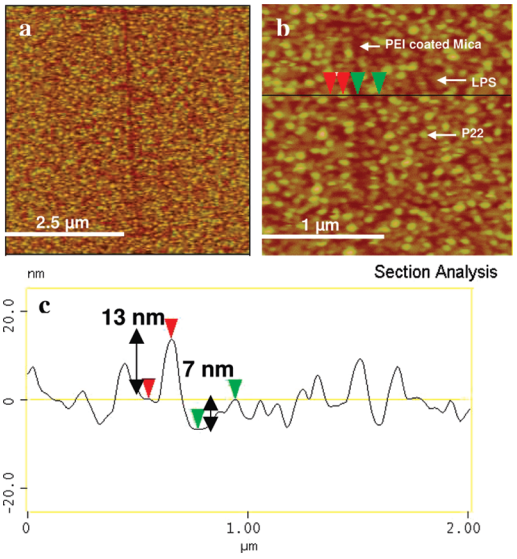

Figure 5. In-situ AFM height images of (a) P22 adsorbed on the LPS bilayer (z range = 50 nm). (b) A magnified image showing P22 found only on top of the LPS domain and not on the bare mica substrate (z range = 50 nm). (c) The cross-sectional height profile along the line in part b showing the LPS bilayer thickness to be 7 nm and the P22 height to be 13 nm.

compressive force greater than 0.1 nN during image capturing. The bilayer thickness estimated from the AFM force curves is within the reported LPS molecular chain length range, that is, 2.5 nm long lipid A, 2.5 nm core, and O antigen portion with length range of 1.3−40 nm.[74]

Our data show that P22 readily adheres to the substrate-supported LPS bilayer. A 100 μL portion of freshly prepared 10^{10}−10^{12} pfu/mL P22 solution was pipetted on the supported LPS surface. The surface was rinsed 3 times with deionized water after 15 min of incubation at room temperature. The surface was imaged in liquid tapping mode in deionized water. Figure 5a shows that the surface morphology after exposure to P22 is uniform over the micrometer range. Three regions (marked by arrows) can be identified according to their characteristic height values in Figure 5b. The darkest region is assigned to the mica substrate with an adsorbed PEI layer, that is, the background. The region with medium height is attributed to the LPS bilayer domain. Its height from the background was determined to be 7.0 ± 0.6 nm (Figure 5c). The brightest region consists of individual particles of P22 whose height and diameter are 14 ± 4 and 77 ± 11 nm, respectively. The particle diameter was measured at the half-maximum height in order to minimize tip

(74) Amro, N. A.; Kotra, L. P.; Wadu-Mesthrige, K.; Bulychev, A.; Mobashery, S.; Liu, G. Y. *Langmuir* **2000**, *16* (6), 2789−2796.

convolution. For comparison, the size of P22 is reported to be 70 nm by cryo TEM.[44] The P22 surface coverage on the supported LPS bilayer was approximately $(45 \pm 5)/\mu m^2$. On the other hand, P22 surface coverage on APTMS-functionalized glass substrate with and without EDC/NHS was reported to be $(40 \pm 4)/\mu m^2$ and $(7 \pm 3)/\mu m^2$, respectively, under similar deposition conditions.[30] It shows that the stereospecific noncovalent binding between supported LPS and P22 is as or stronger than the covalent amide bond via the EDC/NHS route. It is evident that LPS molecules in the supported bilayer retain sufficient mobility to interact with the binding pocket of the gp9 protein.

The immobilized LPS bilayer enables precise and reproducible measurements of molecular recognition forces between P22 and LPS as opposed to measurements using the whole bacterial cell. The binding affinity between P22 mounted on the AFM tip and the supported LPS bilayer on PEI-modified mica was determined by analyzing the retraction force curves measured at different force loading rates, pH, and temperature. Typical retraces of force distance cycles showed a sawtooth pattern with multiple force minima (Figure 6a). The sawtooth force profiles, commonly observed in SMFS studies of ligand−receptor pairs, indicate sequential rupture of different gp9−LPS pairs with each sharp transition corresponding to a rupture event involving a single or multiple gp9−LPS bonds. On the other hand, when we blocked the P22 binding ligands with LPS by immersing P22-functionalized AFM probe in LPS solution, the probe no longer exhibited the attractive interactions with the supported LPS bilayer (Figure 6b). This demonstrates that the multimodal attractive force profile is due to the specific ligand and receptor interaction between P22 and LPS. The unbinding forces are compiled from the local force minima into a force histogram. Figure 6c shows the unbinding force histogram obtained from ~200 force curves between P22 and LPS measured in deionized water (27 °C, pH = 5.5) at a force loading rate of 12 000 pN/s. Distinct force maxima were identified by fitting the force curve with the Gaussian function: 72 ± 9, 130 ± 17, 206 ± 14, and 279 ± 12 pN. The discrete unit force between the ligand and receptor pair was estimated by the common denominator to be ~70 pN. The histogram excluded the force curves that did not exhibit any force spikes. Approximately 20% of the force curves measured between the P22-functionalized probe and the supported LPS bilayer did not exhibit unbinding force transitions, while 90% of the force curves measured with the excess LPS deposited on the probe did not exhibit any unbinding force transitions. It is unlikely that LPS molecules were pulled out of the bilayer because we did not observe any changes in rupture force curves with time. If this were the case, one would expect LPS to continue blocking P22 binding sites−resulting in the disappearance of attractive force minima in subsequent measurements.

The force curves also displayed characteristic separation length between force minima, which was estimated to be in the range 8−17 nm. This pull-off distance or rupture length is commonly associated with stretching of macromolecules (*e.g.*, PEG spacers) by pull-off or adhesion force due to higher elasticity of the macromolecules as compared to the cantilever. In our case, because of the short LPS molecule, relative to those polysaccharides used by others, as well as the expected coupling of LPS stretching (higher contribution) and gp9 stretching (less contribution), we are unable to fit the force versus distance curves with known single chain deformation models, such as the FJC model.

The ligand−receptor unbinding force is a function of the force loading rate. We found similar behavior for the unbinding force between P22 and LPS as shown in Figure 7. The rupture force, F, is a linear function of the logarithm of the force loading rate, r_f between P22-modified AFM probe and the LPS bilayer. The force loading rate was varied between 2100 pN/s and 14 000 pN/s.

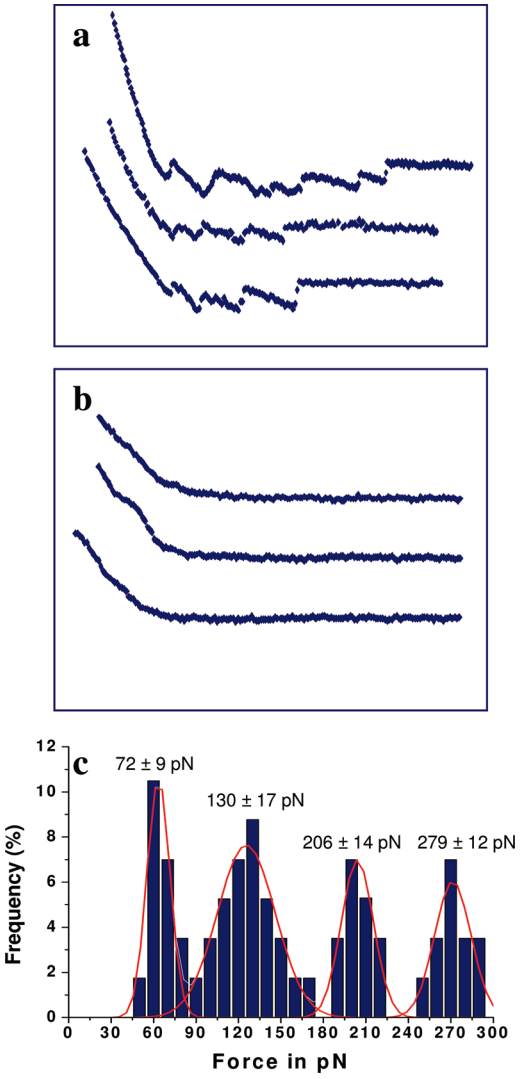

Figure 6. (a) Force vs distance curves during retraction of P22-modified AFM probe from the substrate-supported LPS bilayer measured in deionized water. (b) Force vs distance curves during retraction of P22-modified AFM probe from the substrate-supported LPS bilayer when the P22 binding sites were blocked by excess LPS. (c) Unbinding force histogram with Gaussian fittings.

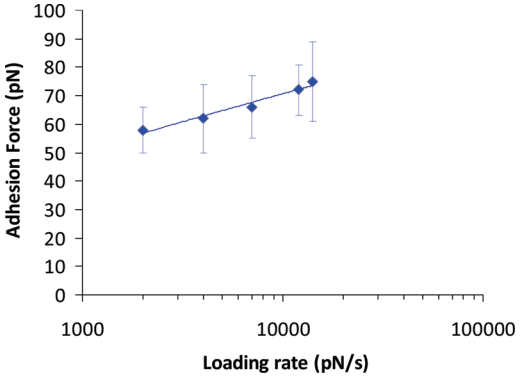

Figure 7. P22−LPS unbinding force dependence on the force loading rate and the fit to the Bell model.

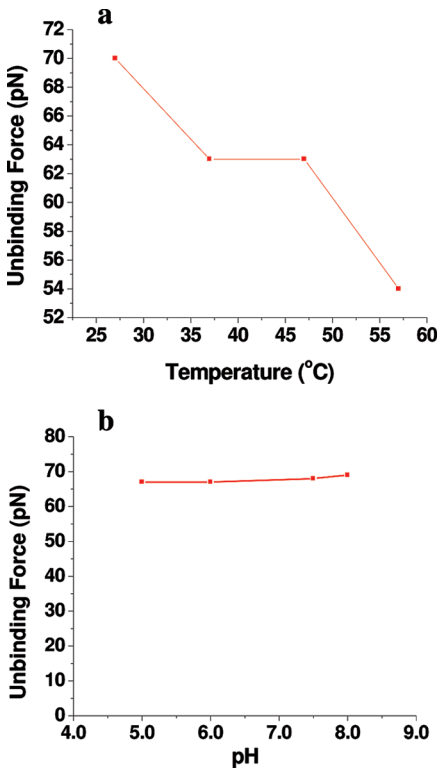

Figure 8. (a) P22−LPS unbinding force as a function of temperature. (b) P22−LPS unbinding force as a function of pH.

The robustness of bacteriophages against environmental stresses such as pH and temperature variations makes them attractive replacements of immunosensors.[75−77] The retraction force curves between P22-functionalized probes and supported LPS bilayers were measured at different temperature values, 27, 37, 47, and 57 °C while pH was maintained at 7.4 and the loading rate was kept constant at 12 000 pN/s. Figure 8a shows the unit unbinding force values as a function of temperature. The unbinding force decreases with increasing temperature at an average rate of 0.7 pN/°C. But even at the highest temperature measured, 57 °C, the unbinding force between P22 and LPS is still significant at more than 50 pN. When the unbinding force was measured at different pH values, it remained constant when pH was changed from 5 to 8 (Figure 8b).

Next, we examine P22 robustness against drying. In our earlier study we demonstrated that after rehydration 40−60% of P22 particles maintained their binding affinity to *S. typhimurium* after they were kept in the dry state for 7 days.[30] Similarly, the P22-modified AFM tip was left drying in a laboratory atmosphere for 7 days, rehydrated, and its interaction with the LPS bilayer was measured. We found that among 200 force curves ~40% of the curves displayed no adhesion. Among the force curves that did exhibit adhesion minima, the unit unbinding force was determined to be 65 pN from the force histogram in Figure 9 while the pH was maintained at 5.5 and the force loading rate was maintained at 12 000 pN/s. In addition, there were fewer multiple interactions indicating loss of gp9 protein activity.

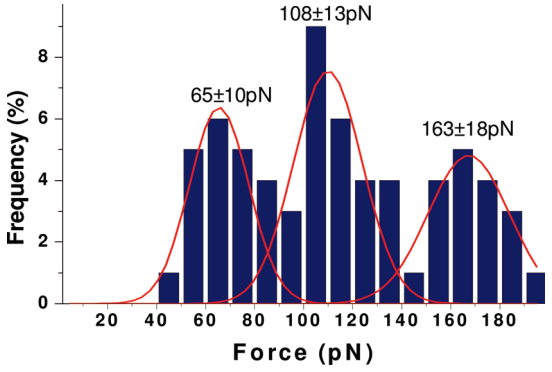

Figure 9. Unbinding force histogram measured in deionized water between P22-modified AFM probe and the LPS bilayer. The probe was dried for 7 days before the measurements. The histogram was obtained from ~200 force curves. The histogram was fitted by the Gaussian distribution.

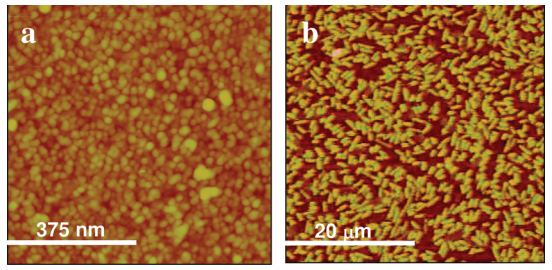

Figure 10. (a) AFM height image of gp9 protein immobilized on COOH-terminated silanized glass (z range = 30 nm); (b) AFM height image of *S. typhimurium* deposited on gp9 layer (z range = 600 nm).

Alternatively, gp9 proteins were isolated from phage P22 and chemically conjugated to the AFM probe. The direct attachment of the gp9 protein allows control of the ligand orientation on the surface and higher ligand density. The N terminus of the gp9 protein reacts with the COOH-terminated carbosilane monolayer assisted by the EDC and NHS chemistry thus exposing the C-terminus for binding to the LPS. The immobilized gp9 protein layer on a silanized glass substrate was imaged by AFM (Figure 10a). Individual gp9 proteins are shown in the AFM image as particulate objects. The height and diameter of the individual particles were estimated from the sectional analysis to be 4.0 ± 0.5 and 17 ± 3 nm, respectively. For comparison, others reported the gp9 diameter to be 3.5−8.0 nm.[43] The increase in the apparent gp9 lateral dimension is expected and is due to AFM probe convolution as well as flattening of the protein molecule upon surface adsorption and drying. From the AFM images, we calculated gp9 protein density to be ~4000/μm^2, via this direct chemical conjugation method. This ligand density value is more than 10 times the value obtained by P22 immobilization, 240/μm^2. The gp9 density via P22 immobilization was calculated by assuming the maximum 6 gp9 proteins per P22 particle and 40 P22 particles per μm^2. The gp9 layer was stable against AFM scanning in the tapping mode in air. The gp9-modified glass substrate was placed in a well filled with 100 μL of freshly prepared *S. typhimurium* culture. Figure 10b shows high coverage of *S. typhimurium* on the gp9 modified substrate. Approximately 450 *S. typhimurium* bacteria were captured by the gp9 substrate on a 4 × 4 μm^2 area, which is ~80% more than what we obtained on P22-modified substrate under identical conditions.

Experiments were also conducted to examine the selectivity of the bacteria with the gp9 coating. The deposited amount of

(75) Raven, N. D. H.; Munster, A. P.; Sharp, R. J. Characterization of thermus bacteriophage YB10. XIV International Congress of Microbiology, Manchester, England, September, 1986.
(76) Sharp, R. J.; Ahmad, S. I.; Munster, A.; Dowsett, B.; Atkinson, T. *J. Gen. Microbiol.* **1986**, *132* 1709−1722.
(77) Zillig, W.; Reiter, W. D.; Palm, P.; Gropp, F.; Neumann, H.; Rettenberger, M. Viruses of Archaebacteria. *The Bacteriophages*; Calendar R., Ed.; Oxford University Press: Oxford, 1988; Vol. 1, p 517.

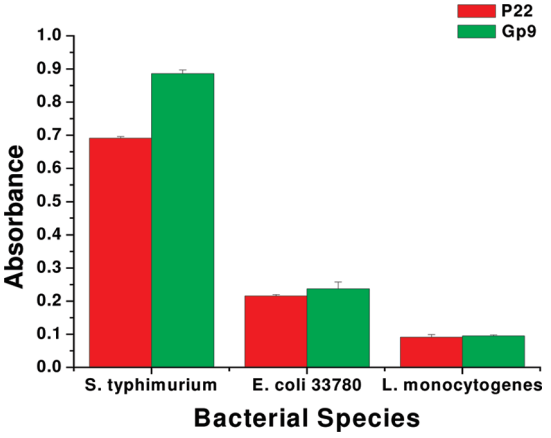

Figure 11. ELISA results showing the difference in binding affinity among *S. typhimurium*, *E. coli*, and *L. monocytogenes* on gp9- and P22-modified silanized glass substrates.

S. typhimurium is compared to those of *E. coli* (strain 33780), a Gram-negative bacterium with weaker affinity to gp9, and L. monocytogenes, a Gram-positive bacterium without the O-antigen LPS outer layer. Figure 11 shows the ELISA results of the comparison among different bacterial adsorption on gp9 protein and P22 particles. ELISA was repeated on three different samples for each bacterium for gp9 and P22 separately. The results show a clear discrimination of different bacteria with gp9 and P22. Because of the higher density of gp9 on the substrate as compared to the P22 density, almost 30% higher absorbance was obtained with gp9 coating.

The AFM force curves between gp9 immobilized on an AFM probe and the LPS bilayer are similar to those between P22 and LPS as shown in Figure 6a. The unbinding force histogram obtained from 250 force curves between gp9 and LPS measured in deionized water (T = 27 °C, pH = 5.5) and at 12 000 pN/s reveals a multimodal distribution of unbinding forces with the first three maxima at 70, 135, and 200 pN. Thus it also gives discrete molecular interactions with a single bond value of 70 pN. The rupture distance using gp9 has a much wider distribution probably because it is bound directly to a hard surface—the AFM probe. Further investigation using a flexible spacer between gp9 and the AFM probe surface will be able to more accurately distinguish nonspecific from specific interactions.

4. Discussion

We have shown that direct attachment of P22 as well as gp9 proteins to AFM probes allow the measurements of discrete unbinding forces between the protein−carbohydrate pair. This conclusion is supported by (1) clustering of data around specific unbinding force values that are also quantized, (2) the fit of unit force values to the Bell model, (3) the lack of adhesion between probe and surface when the binding proteins are blocked by LPS molecules, and (4) strong adsorption of P22 on a supported LPS bilayer and *S. typhimurium* on an immobilized gp9 monolayer. Because of the large size of P22, it is conceivable that poly(ethylene glycol) (PEG) tethers of a few tens of nanometers in length will not make a significant difference in force rupture distances measured using P22-modified AFM probes. In the case of immobilized gp9 proteins, future measurements with PEG tethers may be necessary to clearly distinguish nonspecific binding from specific binding on the basis of the rupture distance correlation with the spacer length. Our evidence also shows that LPS in the substrate-supported bilayer is free to bind to gp9 proteins. This could be because LPS extends away from the lipid core into the solution, which permits more free volume for its interaction. In fact, the extension of LPS into the surrounding environment is believed to contribute to cell recognition in many biological processes involving LPS. On the other hand, membrane proteins more closely embedded in the lipid core are known to lose their biological activities in the supported bilayer without a polymeric cushion.

The force curves between P22 (or gp9) and LPS show multiple peaks, which is indicative of multivalent interactions between the pair. The second, third, and fourth most common forces values are approximately 2×, 3×, and 4× of the lowest most common force value, 72 pN, taken at 12 000 pN/s. The quantized nature of the forces is consistent with multiple bond ruptures with the lowest rupture force corresponding to the monovalent bond. The force value is reduced by 10 pN when the experiments were done in 5 mM Hepes and 25 mM KCl instead of deionized water. Salt has the effect of reducing nonspecific electrostatic interaction.[78,79]

The force spectra were analyzed using the Bell model by plotting the rupture force F as a logarithmic function of the force load rate r_f.[48,80] The Bell model describes the bond strength of noncovalent bonds to be a function of r_f. The loading rate dependence is related to the reduction in the lifetime of a noncovalent bond when a force is applied because of thermal activation. Consequently F increases with increasing r_f. The value of barrier position x can be obtained from the force scale or slope, $f_B = k_BT/x$, where k_B is Boltzmann constant and T is the temperature. The barrier height E_b can be obtained from the intercept of the force at the logarithmic loading rate axis according to eq 1.[80,81]

$$E_b = k_BT\left[\ln\left(\frac{k_BT}{t_Dx}\right) - \ln(r_f)\right] \quad (1)$$

f_B was determined to be 8 pN, which gives a barrier position x = 0.5 nm. The barrier height E_b was calculated to be 22.2 k_BT or 55.5 kJ/mol from eq 1 by assuming a relaxation frequency $1/t_D$ of 1×10^{-9} s^{-1}.[80,81] While analyzing the rupture forces the damping and frictional effects were neglected because it has been shown[81] that these forces are insignificant as compared to the measured forces. The barrier height value is in the range of known values the ligand−receptor interactions[6,80−83] and consistent with the activation energies for P22 TSPs.[20,41] The binding free energy for TSP and O-antigen of *S. typhimurium* was reported to be 30 kJ/mol.[41] In another study,[20] using isothermal titration calorimetry the values of enthalpic barriers for the association and dissociation of oligosaccharide to P22 were found to be 50 and 100 kJ/mol, respectively. It should be noted while our experimental values of the unit unbinding forces between individual gp9 proteins and LPS molecules are comparable to the antibody−antigen interactions within the SMFS type of measurements, the SMFS force values may not compare directly with equilibrium ligand−receptor binding affinities. The affinities are measured using free

(78) Willemsen, O. H.; Snel, M. M. E.; Kuipers, L.; Figdor, C. G.; Greve, J.; De Grooth, B. G. *Biophys. J.* **1999**, *76* (2), 716−724.
(79) Bowen, W. R.; Hilal, N.; Lovitt, R. W.; Wright, C. J. *J. Colloid Interface Sci.* **1998**, *197* (2), 348−352.
(80) Merkel, R.; Nassoy, P.; Leung, A.; Ritchie, K.; Evans, E. *Nature* **1999**, *397* (6714), 50−53.
(81) Williams, P. M.; Moore, A.; Stevens, M. M.; Allen, S.; Davies, M. C.; Roberts, C. J.; Tendler, S. J. B. *J. Chem. Soc., Perkin Trans. 2* **2000**, (*1*), 5−8.
(82) Idiris, A.; Kidoaki, S.; Usui, K.; Maki, T.; Suzuki, H.; Ito, M.; Aoki, M.; Hayashizaki, Y.; Matsuda, T. *Biomacromolecules* **2005**, *6* (5), 2776−2784.
(83) Allen, S.; Chen, X. Y.; Davies, J.; Davies, M. C.; Dawkes, A. C.; Edwards, J. C.; Roberts, C. J.; Sefton, J.; Tendler, S. J. B.; Williams, P. M. *Biochemistry* **1997**, *36* (24), 7457−7463.

species in solution while in SMFS the rupture forces are measured between surface-attached ligand and receptor pairs.[84−86]

5. Conclusions

This paper reports methods to immobilize phage P22 and its tail spike protein gp9 on AFM probes using bioconjugation chemistry. The direct attachment of gp9 proteins facilitates the proper orientation of the ligand for binding and increases its surface coverage. The ability of the surface-immobilized P22 and gp9 proteins to recognize LPS on the surface of Gram-negative bacterium *S. typhimurium* is demonstrated by AFM imaging and SMFS measurements. The results show that the gp9−LPS interaction can be measured using a homogeneous LPS bilayer instead of the whole bacterial cell of *S. typhimurium*. The forces were measured at different force loading rates as well as different environmental conditions, including temperature, pH, and humidity. The binding energy barrier was determined to be 55 kJ/mol by fitting the force data with the Bell model. The molecular recognition forces between phage and bacterial cells reach the same range as antibody−antigen forces. However, compared to antibodies, phages are less fragile and less sensitive to environmental stresses, such as pH and temperature fluctuation, which make them attractive substitutes to immunosensors. The phage-based sensors could provide longer field life for the detection of toxins, bacteria, and spores. In addition, the new phage display technology offers a billion clone libraries of recombinant phages for high-throughput detection.

Acknowledgment. We acknowledge the National Science Foundation (CBET-0553533, CBET-0619528, and CBET-0755654) and Wayne State University Graduate School Graduate Research Assistantship and Rumble Fellowship (Handa). We thank the laboratory of Dr. Gregory Auner for providing CDDMS for AFM probe functionalization.

(84) Chang, K. C.; Hammer, D. A. *Biophys. J.* **1999**, *76* (3), 1280−1292.
(85) Riper, J. W.; Swerlick, R. A.; Zhu, C. *Biophys. J.* **1998**, *74* (1), 492−513.
(86) Zhu, C. *J. Biomech.* **2000**, *33* (1), 23−33.